

## Design method and performance comparison of plenum and volute delivery systems for radial inflow turbines

J. A. Keep<sup>1</sup> and I. J. Jahn<sup>1</sup>

<sup>1</sup>School of Mechanical and Mining Engineering  
University of Queensland, Queensland 4072, Australia

### Abstract

Radial inflow turbines are the preferred architecture for energy extraction from the organic Rankine cycle and the supercritical CO<sub>2</sub> Brayton cycle at smaller scales. For such turbines it is possible for fluid to be delivered to the first stage by either a volute or plenum delivery system. For high pressure supercritical CO<sub>2</sub> turbines, there are no fully documented fluid delivery systems in literature and it remains unclear as to which architecture results in higher performance with the highly dense working fluid. The aim of this paper is to present a performance comparison between a new plenum based fluid delivery system and conventional volute for a 100 kW supercritical CO<sub>2</sub> radial inflow turbine. Numerical simulations of the fluid delivery systems are conducted and compared in terms of flow uniformity, total pressure loss and entropy rise.

It is demonstrated that fluid can be delivered to the stator vanes with a plenum style inlet for a radial inflow supercritical CO<sub>2</sub> turbine without re-circulation regions and minimal total pressure loss. Entropy rise for the plenum is reduced more than tenfold in comparison to the volute, however fluid velocities are not matched and there is a periodic variation in in velocity generated by the multiple inlets.

### Introduction

An efficient embodiment of the supercritical CO<sub>2</sub> Brayton cycle is a key enabler for the development of concentrating solar power on a scale of less than 10 MW [4]. Radial inflow turbines that satisfy these ratings are under 500 mm in rotor diameter with comparatively small blade inlet heights. This presents a unique combination of small geometry and very high inlet duct Reynolds number ( $3 \times 10^6$ , or approximately 100 times greater than air turbomachinery of similar scale), therefore the optimal design of these turbines remains unclear.

For the efficient operation of a radial inflow turbine stage, fluid needs to be uniformly supplied to all stator nozzle guide vanes with uniform pressure and a matched tangential velocity component. Volute are the preferred method to provide the highly tangential flows as typically required in conventional radial inflow turbines. An alternative to this are plenum style inlets. For the present application of radial inflow turbines, it is unclear as to which is the preferred method of fluid delivery.

Using conventional machining methods, the relative stack-up of tolerances is increased at small scale, leading to the potential for greater deviation from nominal design in components. A plenum fluid delivery system is of interest in this design space, as it is less dimensionally critical than a volute.

The aim of this paper is to present a performance comparison between a plenum based fluid delivery system and conventional volute for a supercritical CO<sub>2</sub> radial inflow turbine with operating conditions described in table 1. These conditions are representative of small scale applications and preferred cycle conditions targeted at a concentrated solar thermal application [3].

Operating Conditions	Value	Parameter	Value
Power	100 kW	$r_1$	32.40 mm
Total Pressure	20 MPa	$Z_1$	1.25 mm
Total Temperature	833 K	$\alpha_1$	80.91 <sup>0</sup>
Mass Flow Rate	1 kg s <sup>-1</sup>		

Table 1: Turbine operating conditions and stator geometry parameters

### Design

The aerodynamic objective of a fluid delivery system in radial turbomachinery is to deliver a uniform flow from the delivery pipe to the stator inlet. If a high velocity stream is to be delivered to the stator inlet, it is important for the flow to match the stator blade angle in order to minimise incidence losses. By contrast, if a low velocity stream is delivered, incidence is of less importance.

Inlet pipe are sized such that Mach number is below 0.1, or less than the 30 m s<sup>-1</sup> as recommended by Southwest Research Institute [6]. Stator inlet constraints and total inlet conditions are derived from a 100 kW supercritical CO<sub>2</sub> mean-line design presented by Qi et.al. [8] and listed in table 1.

### Plenum

The primary advantage of a plenum fluid delivery system is the ability to employ a cross section of constant shape, allowing manufacture in two halves and simplifying assembly of a high pressure turbine casing. The selected cross section satisfying these requirements is illustrated in figure 1.

An important consideration with a plenum inlet is jet impingement into a quiescent body of fluid. In the traditional design of axial flow turbomachinery inlet plenums, this appears to be done with the use of diffusers [7]. In the case of supercritical CO<sub>2</sub>, the characteristic design of diffusers requires a much larger space claim than that for air [5], and it would not be practical to incorporate such features in a compact plenum. An alternative to manage the high velocities at the pipe outlet is to offset inlet pipes as shown in figure 2 thus inducing tangential flow in the plenum. This also avoids localised impingement of the incoming flow on the stator. A asymmetric plenum cross-section has been selected in order to avoid toroidal vortices from establishing [2]. Feature sizes of the plenum design are minimised in order to limit system volume and are listed in table 2.

Feature	Value	Feature	Value
$Z_0$	15.20 mm	$A_0$	57 mm <sup>2</sup>
$L_0$	15 mm	$A_{in}$	181 mm <sup>2</sup>
$L_1$	5 mm	$r_0$	45 mm
$b$	50 mm	$t$	4 mm
$\gamma$	40 <sup>0</sup>		

Table 2: Geometric parameters of delivery systems

### Volute

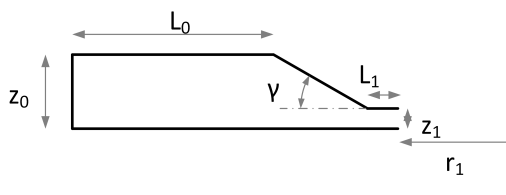


Figure 1: Section view of plenum

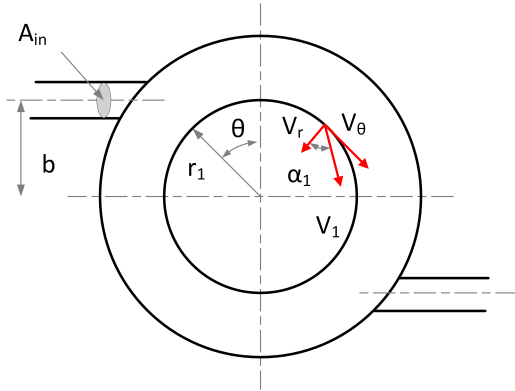


Figure 2: Plan view of plenum

The volute geometry is developed based on the assumption of conservation of angular momentum. With this assumption, the following relationships exist for exit flow angle and area[7].

$$\tan \alpha_1 = \frac{\rho_1 (A_1 / r_1)}{\rho_0 (A_0 / r_0)} \quad (1)$$

$$\frac{A_\theta}{r_\theta} = \frac{\dot{m}}{\text{const.} \cdot \rho_\theta} \left(1 - \frac{\theta}{2\pi}\right) \quad (2)$$

Observing equation 1 and assuming constant density within the volute, it can be seen that the outlet flow angle ( $\alpha_1$ ) is dictated by the inlet area ( $A_0$ ) and radius ( $r_0$ ). Assuming constant density, in order for a constant mass flow to be delivered to the stator stage a linear decrease in  $A_\theta / r_\theta$  with  $\theta$  is required. Using the approximation, of constant volute radius ( $r_\theta$ ) this gives a linear reduction in volute sectional area ( $A_\theta$ ) with  $\theta$ . The plan shape of the volute as illustrated in figure 4 is mathematically described by several logarithmic spirals. The tongue thickness, ( $t$ ) has been prescribed to limit thermal loads and fatigue. The inter space between the inner edge of the scroll and the stator has been set using design guidelines presented in Aungier[2], to be greater than  $1.05 r_1$ . This minimises non-uniformities introduced by the tongue. Furthermore to avoid the development of two opposing toroidal vortices, which increase losses, the volute outlet is offset with a circular cross-section as illustrated in figure 3.

### Modelling

Both geometries are modeled in three dimensions. The volute is modeled in its entirety from inlet pipe to stator inlet passage. Owing to rotational symmetry, the plenum is modeled as a half circumferential section. The geometries were constructed using CAD and meshed using ANSYS meshing 17.0.

Inlet pipes to each geometry are modeled with a length greater than five times the inlet diameter in order to minimise inlet effects on the area of interest. To ensure comparability, total inlet cross sectional area of geometries is matched.

The ANSYS CFX 17 solver is used for calculations [1]. Thermodynamic and transport properties are incorporated into the CFD solver through the built-in thermophysical library for CO<sub>2</sub>.

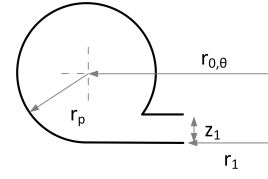


Figure 3: Section view of volute

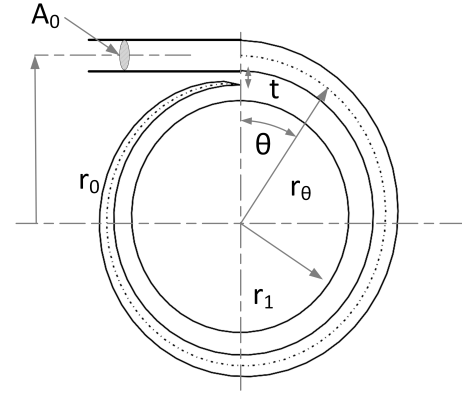


Figure 4: Plan view of volute

Boundary conditions are derived from a 100 kW supercritical CO<sub>2</sub> mean-line design presented by Qi et.al. [8], and specified in table 3. For all simulations, the SST  $k - \omega$  turbulence model is used with a 5% turbulence intensity at the inlet in line with simulations conducted by Monje et.al. [5].

Surface	Type	Value
Inlet	total pressure	20.0 MPa
Outlet	static pressure	17.15 MPa
Upper and lower	no-slip wall	N/A
Edges	rotational periodicity	N/A

Table 3: Boundary conditions for CFD simulation

### Meshing

Unstructured meshes are used for both plenum and volute geometries. A grid dependency study comparing three meshes was completed on the plenum geometry, comparing mass flow averages for inlet and outlet of total enthalpy and entropy difference and mass flow. The nominal mesh has approximately 90000 nodes. Results from the dependency study are presented in table 4, confirming grid independence. The nominal mesh was selected for further analysis. The same mesh settings were utilised for automated meshing of the volute geometry resulting in a mesh with approximately 640000 nodes.

The plenum mesh was refined using 100 inflation layers to resolve the wall boundaries. This resulted in a typical near wall cell height of 0.2 mm and a  $y^+$  in the range of 1000 to 10000. This is larger than the recommended  $y^+$  range for the turbulence model ( $30 < y^+ < 300$ )[1], however finer meshes would prevent solution convergence due to flow instabilities at the exit of inlet pipes. For the volute mesh convergence was achieved with a first layer height closer to the desired value with  $6 \times 10^{-3}$  mm. Clustering was employed in regions of anticipated flow separation and high pressure gradients. Visualisation of entropy gradient over the domain was used to verify clustering.

### Results

Mesh	$\Delta s$ (J/kg.K)	$h_{0,total}$ (kJ/kg)	$h_{1,total}$ (kJ/kg)
coarse	4.81	8385.1	8385.1
nominal	4.70	8385.1	8385.1
fine	4.25	8385.1	8385.1

Table 4: Results from grid dependence study for plenum mesh, refinement ratio 2.0

Parameter	Volute	Plenum
$h_{1,total}$ (kJkg <sup>-1</sup> )	8385.11	8385.11
$\Delta s$ (Jkg <sup>-1</sup> K <sup>-1</sup> )	8.06	0.49
$P_1$ (MPa)	17.15	19.72
$\Delta P_{1,total}$ (MPa)	0.83	0.05
$\dot{m}$ (kg s <sup>-1</sup> )	1.11	1.11
$\eta_{isentropic}$	73 %	80 %

Table 5: Comparison of exit flow properties for geometries

Utilising the boundary conditions from table 3, exit mass flow for the plenum and volute geometries are not in close agreement. This is attributed to the difference in effective outlet flow area ( $A_{eff} = \frac{A_{actual}}{\cos \alpha_1}$ ) and difference in total pressure losses between the two geometries. To allow comparison between the geometries, exit static pressure for the plenum simulations was adjusted until mass flow was matched to the volute simulation. The plenum simulation was adjusted owing to the smaller mesh. Exit flow properties for each geometry are compared in table 5. The plenum maintains higher total pressure with lower entropy rise than the volute, and higher isentropic efficiency.

To visualise flows, and potential regions of re-circulation and loss generation, streamline plots and pressure contours are shown in figures 5 and 6. These plots show no significant regions of re-circulation or secondary flow. Both geometries display the highest rate of entropy generation in the contraction close to the outlet. The rate of entropy generation in the volute is significantly larger in this region than for the plenum, with further entropy generation in the region of the tongue. To examine outlet flows in greater detail, azimuthal variation in outlet velocities are compared in figure 7. The volute delivers a higher velocity magnitude with a larger tangential component. Plenum radial and tangential velocities exhibit two characteristic peaks corresponding to the two inlets. For the volute, in the region of the tongue and for approximately 120° thereafter there is fluctuation in outlet velocity, then it remains relatively constant. Examining the outlet flow angle ( $\alpha_1$ ) in figure 8, it can be seen that the volute delivers close to design requirement of  $\alpha_1$  with minor deviation in the region of the tongue. This is not the case with the plenum where large fluctuations in flow angle are present, and the mean flow angle is significantly lower than the design requirement.

## Discussion

For the scale considered, the numerical comparison of the plenum and volute show a significantly superior performance of the plenum. Entropy generation and total pressure loss are both reduced by a factor of 16. Inspection of the entropy generation shows that this difference can be attributed to lower velocities and the elimination of the area discontinuity in the vicinity of the volute tongue.

However the exit velocities delivered by the plenum are substantially lower at 61 ms<sup>-1</sup> compared with 192 ms<sup>-1</sup> and exit flow direction has an increased radial component. The plenum exit velocity magnitude is almost invariant, but the flow angle varies by  $\pm 16\%$ . The much reduced velocities at the plenum exit and the low variations in tangential velocity suggests a different approach to stator design. For example by using stator

blades that are tolerant to variations in incident flow and optimised for flow acceleration and flow turning, desired stator outlet conditions can be attained. Alternative solutions to increase the tangential velocity component are to increase the offset of the plenum inlet pipes ( $b$ ) or to reduce the inlet area ( $A_{in}$ ). Similarly angular periodic variation in flow angle ( $\alpha_1$ ) can be smoothed through the addition of additional feeder pipes. However these approaches are not preferred due to additional complexity and limit space that is available in such small turbine casings.

Close inspection and comparison of the different flow fields show that the design methods deliver a generally smooth flow. For both geometries, no significant toroidal vortices are generated, showing that the employed geometries operate to design intent. Additional scope exists to further enhance performance through better blending of the inlet pipes and smoothing of sharp edges, avoidance of flow area discontinuities and to develop stator vanes optimised for the respective flow conditions.

The current work studied a 100kW scale turbine (inlet radius < 50mm). It is anticipated that for larger systems 1 MW to 10 MW the performance benefits of the plenum become less pronounced, but that significant manufacturing advantages remain. Furthermore the plenum requires equal or less space than a compact volute. Considering this in conjunction with the much simplified manufacturing, this is an additional advantage for the design of higher pressure turbine casings.

This work has shown that for radial inflow turbomachinery operating with sCO<sub>2</sub>, which results in very high stage Reynolds numbers for small geometries, a plenum is the preferred fluid delivery system, if used in conjunction with nozzle guide vanes.

## Conclusions

Both fluid delivery systems deliver a generally smooth flow with no regions of secondary flow. The numerical comparison of the plenum and volute show a significantly superior performance of the plenum with an entropy rise and total pressure loss of approximately 16 times less than the volute. This difference can be attributed to the higher velocities in the volute, and higher isentropic efficiency. Comparing variation in outlet velocity, it can be seen that the plenum does not deliver the requisite tangential component of velocity and possess a more sustained variation with azimuthal angle when compared to the volute. In order to better understand the impact of stator stage interactions with a plenum delivery system, it is suggested that further simulation work be performed with the inclusion of stator vanes.

## Acknowledgments

This research was performed as part of the Australian Solar Thermal Research Initiative (ASTRI), a project supported by the Australian Government.

## References

- [1] ANSYS Academic Research, 2015, ANSYS Release 16.1, Theory Manual, Inc., Canonsburg, P.A..
- [2] Aungier, R. H., *Turbine aerodynamics : axial-flow and radial-inflow turbine design and analysis*, ASME, 2006.
- [3] Dyreby, J., Klein, S., Nellis, G. and Reindl, D., Design considerations for supercritical carbon dioxide brayton cycles with recompression, *Journal of Engineering for Gas Turbines and Power*, **136**, 2014, 101701.

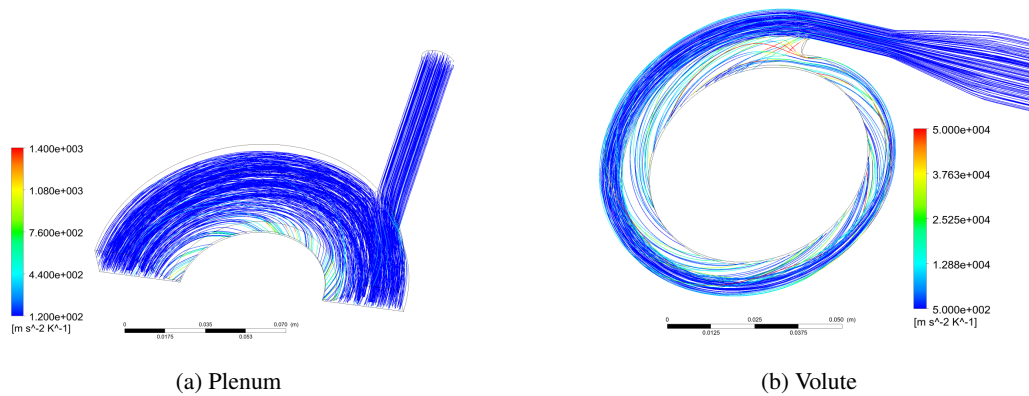


Figure 5: Streamline plots coloured by static entropy gradient to highlight locations of loss generation.

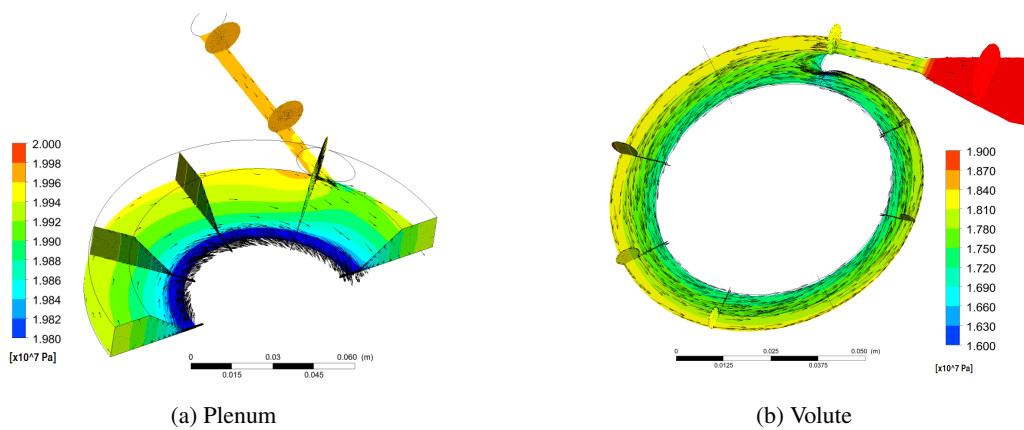


Figure 6: Static pressure contour and vector plots to highlight flows.

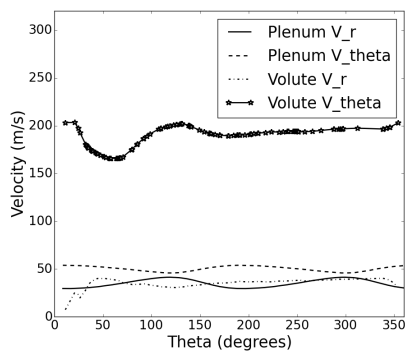


Figure 7: Angular ( $\theta$ ) variation of velocity components at the plenum and volute outlet. ( $V_r$  - radial velocity component,  $V_{\theta}$  - tangential velocity component)

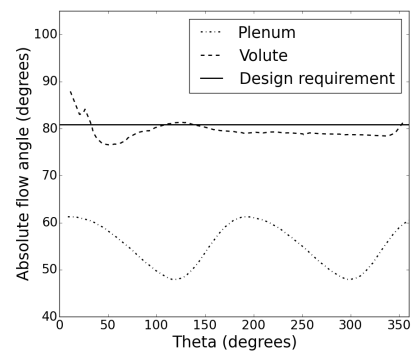


Figure 8: ( $\alpha_1$ ) variation with  $\theta$

[4] Gurgenci, H., Supercritical  $\text{CO}_2$  cycles offer experience curve opportunity to cost in remote area markets, *Energy Procedia*, **49**, 2014, 1157–1164.

[5] Monje, B., Sanchez, D., Chacartegui, R., Sanchez, T., Savill, M. and Pilidis, P., Aerodynamic analysis of conical diffusers operating with air and supercritical carbon dioxide, *International Journal of Heat and Fluid Flow*, **44**, 2013, 542 – 553.

[6] Moor, J., Brun, K., Evans, N., Bueno, P. and Kalra, C., Development of a 1mwe supercritical  $\text{CO}_2$  brayton cycle test loop, in *The 4th International Symposium - Supercritical  $\text{CO}_2$  Power Cycles*, 2014.

[7] Moustapha, H., Zelesky, M. F., Baines, N. C. and Japikse, D., *Axial and radial turbines*, volume 2, Concepts NREC White River Junction, VT, 2003.

[8] Qi, J., Reddell, T., Qin, K., Hooman, K. and Jahn, I. H., Supercritical  $\text{CO}_2$  radial turbine design performance as a function of turbine size parameters, in *Proceedings of ASME Turbo Expo 2016: Turbomachinery Technical Conference and Exposition*, 2016.